How Magnification of the Root-Mean-Square Deviation (RMSD) Value Affects the Convergence Speed of Hopfield Neural Network Classifier

RACHID SAMMOUDA
Department of Computer Science
University of Sharjah
Sharjah, P.O.B. 27272
UAE
rsammouda@sharjah.ac.ae

Abstract: - The Root Mean Square-Deviation (RMSD) or Root Mean Square Error (RMSE) is the frequently used measure of the difference between values predicted by a model or an estimator and the values actually observed from that which is being modelled or estimated. In this paper, we show that the magnification of the RMSE, when used with the classifier Hopfield Neural Network (HNN), may help the network to converge earlier to the same optima reached using the simple RMSE. The segmentation problem of liver pathological images is formulated in energy function as a magnified sum of all neurons' deviations from their actual clusters, and HNN iterates with respect to the winner-takes-all rule in order to minimize the energy function to a local optimum close to the global one. Twenty liver color images were used in this study. Their segmentation results with their corresponding quantitative analysis show that our approach makes the results more reliable for use as input data to a computer aided diagnosis of liver cancer.

Key-Words: - Hopfield Neural Network, Optimization, Mean-Square-Error, Magnification, Segmentation, pathological liver color image

1 Introduction

Artificial neural networks (ANNs) represent a powerful tool for computation and as an alternative to optimization problem solving. They are typically able to solve constrained linear and quadratic programming problems possessing local extremes. Simulation results concerning the approximation capabilities seem quite elaborate, but they still cannot answer all our relevant theoretical questions.

The niche of neural network models is quite wide, ranging from simple system of ordinary differential equations to complex models with some ambiguous multipliers. Most of the neural networks minimize the specific energy or error function. It is not clear, in general, how to construct the corresponding energy function. Up till now, it has been difficult, if not impossible, to encompass such different approaches by unifying theory. It is desirable to gain insight about global convergence, stability and neural architecture of the model with respect to different classes of primal and dual optimization problems [1]. In this paper we use ANNs as optimizer to segment color medical images.

Segmentation is an important step in most applications that use medical image data. For example, segmentation is a prerequisite for quantification of morphological disease manifestations and for radiation treatment planning [2-3], for construction of anatomical models [4], for definitions of flight paths in virtual endoscopies [5], for content-based retrieval by structure [6], and for volume visualization of individual objects [3].

A number of algorithms based on approaches such as histogram analysis, regional growth, edge detection and pixel classification have been proposed in other analyses of medical image segmentation. ANNs have been proposed as an attractive alternative solution to a number of pattern recognition problems [7]. In our previous works [8], we have explored the potential of a Special Case of Hopfield Neural Network (HNN) in segmenting cerebral images obtained using the Magnetic Resonance Imaging (MRI) technique.

Hopfield network for the optimization applications consists of many interconnected neuron elements. The network minimizes an energy function of the form:

$$E = \sum_{K=1}^{N}\sum_{I=1}^{N} T_{KI} V_K V_I - \sum_{K=1}^{N} I_K V_K \quad (1)$$

where N is the number of neurons, V_k is the output of the k^{th} neuron, I_k is the bias term, and T_{kl} is the interconnection weight between the k^{th} and l^{th} neurons. The energy function used in the segmentation problem is slightly different from the one defined by Hopfield and the arguments are given in Amartur, et al.[9].

The results obtained by Sammouda, et al. [8] were preferable to those obtained using Boltzmann Machine (BM) and the conventional ISODATA clustering technique. Additionally, our laboratory has previously shown that HNN is also able to produce crisp segmentation of pathological liver color images [10].

However, in the present study, we have attempted to improve the segmentation process; we found that HNN segmentation results depend strongly on some parameters in the energy function formulating the classification problem and here, we present some of this dependency.

2 Formulation of the Segmentation Problem

The segmentation problem of an image of *N* pixels has been previously formulated as a partition of the *N* pixels among *M* classes, such that the assignment of the pixels minimizes a criterion function [10]. The HNN classifier structure consists of a grid of *N*×*M* neurons with each row representing a pixel and each column representing a cluster.

The network classifies the image composed of *N* pixels with *P* features among *M* classes, in a way that the assignment of the pixels minimizes the following criterion function:

$$E = \frac{1}{2}\sum_{k=1}^{N}\sum_{l=1}^{M} R_{kl}^{n} V_{kl}^{2} + c(t)\sum_{k=1}^{N}\sum_{l=1}^{M} N_{kl} V_{kl} \qquad (2)$$

where R_{kl} is the Mahalanobis distance measure between the k^{th} pixel and the centroid of class *l*. R_{kl} is also equivalent to the error committed when a pixel *k* is assigned to a class *l*.

The index *n* in R_{kl}^{n} is the power or weight of the considered error in the energy function of the segmentation problem, and V_{kl} is the output of the kl^{th} neuron. N_{kl} is a *N*×*M* vector of independent high frequency white noise source used to avoid the network being trapped in early local minimums.

The term *c(t)* is a parameter controlling the magnitude of noise which is selected in such a way as to provide a zero as the network reaches convergence. The minimization is achieved by using HNN and by solving the motion equations satisfying:

$$\frac{\partial U_{kl}}{\partial t} = -\mu(t)\frac{\partial E}{\partial V_{kl}} \qquad (3)$$

where U_{kl} is the input of the k^{th} neuron, and μ(*t*) is a scalar positive function of time, used as heuristically motivated stopping criterion of HNN, and is defined as in [8] by:

$$\mu(t) = t(T_s - t) \qquad (4)$$

where *t* is the iteration step, and T_s is the pre-specified convergence time of the network which has been found to be 120 iterations [8].

The network classifies the feature space, without teacher based on the compactness of each cluster calculated using Mahalanobis distance measured between the k^{th} pixel and the centroid of class *l* as given by:

$$R_{kl} = \left\| X_k - \overline{X}_l \right\|_{\sum_l^{-1}} = \left(X_k - \overline{X}_l\right)\sum_l^{-1}\left(X_k - \overline{X}_l\right) \qquad (5)$$
$$1 \le k \le N \text{ and } 1 \le l \le M$$

where X_k is the *P*-dimensional feature vector of the kth pixel (here *P* = 3 with respect to the RGB color space components), $\overline{X}_l$ is the P-dimensional centroid vector of class *l*, and $\sum_l$ is the covariance matrix of class *l*. The segmentation algorithm is described as follows in our previous work [10]:

- Step 1: Initialize the input of the neurons to random values.
- Step 2: Apply the following input-output relation, establishing the assignment of each pixel to only one class:

$$\text{if } U_{km} = Max\left[U_{kl}(t), \forall l\right] \text{ then } V_{km}(t+1) = 1,$$
$$\text{else } V_{km}(t+1) = 0, \qquad (6)$$
$$1 \le k \le N, \text{ and } 1 \le l \le M$$

- Step 3: Compute the centroid $\overline{X}_l$ and the covariance matrix Σ_l of each class l, respectively, as follows:
-

$$\overline{X}_l = \sum_{k=1}^{N} X_k V_{kl} \Big/ n_l \quad (7)$$

$$1 \le l \le M$$

$$\sum_l = V_{kl}\left(X_k - \overline{X}_l\right)^T \Big/ n_l - 1 \quad (8)$$

where n_l is the number of pixels in class l, and the covariance matrix is then normalized by dividing each of its elements by $\left[\sum_l\right]^{1/p}$.

- Step 4: Update the inputs of each neuron by solving the set of differential equations in (2) using Euler's approximation:

$$U_{kl}(t+1) = U_{kl}(t) + \frac{dU_{kl}}{dt} \quad (9)$$

$1 \le k \le N$, and $1 \le l \le M$

- Step 5: If $t < T_s$, repeat from Step 2, else terminated.

In order to study the effect of the weighted error or distance R_{kl} in the cost function (2), we have provided a simple modification to the above algorithm by considering a fixed random initialization N× M matrix in Step 1. This condition is added to the algorithm in order to make sure that the random field does not have any effect on the generated results.

The RMSD algorithm is simple, robust and most popular algorithm for adaptive filtering applications [11], however, with nonlinear systems like HNN the RMSD may act better with specific values of its parameters. For this, we have varied the variable n (error's weight), in equation (1) the energy function of the segmentation problem to study the effect of varying the main parameter of the RMSD algorithm. Other steps, from Step 2 through Step 5, remain the same.

2.1 Segmentation Results

For this study, a total of 20 liver tissue sections were provided by the pathological division of the National Cancer Center in Tokyo. These sections were obtained by needle biopsy, stained with hematoxylin and then magnified with an optical microscope. Figure 1 shows a true RGB color image of liver tissue of 768×512 pixels. We have used the above described HNN classifier with the image components in the R.G.B color space. The number of classes is fixed to five, based on medical information. These classes are the contour of the image, the cell's nuclei, the cytoplasm, the fibrous tissues, and the class of both blood sinus and fat cells.

Figure 2 shows the curves of the HNN energy function during the segmentation of the sample shown in Figure 1, with Ts values between 30 and 120 iterations. Similar curves were obtained for the rest of the images in the dataset, as illustrated in Figure 2. The curve corresponding to Ts = 120 iterations gives the optimal solution, as was found with MRI data [7].

Figure 3 shows different curves of the optimization of the energy function of the segmentation of the sample shown in Figure 1 using HNN with the above modification (Step 1) with respect to different values of the variable n in equation (2). Based on the findings shown in Figure 2, the pre-specified convergence time of HNN is fixed to Ts = 120 iterations.

However, we can clearly see from Figure 3 that with a higher value of n in Equation (2), the same or close convergence point is reached in half the time of the one reached with n = 2 and Ts = 120 iterations. So, this raises the following question: what is the type of relation between the variable n in (2) and the pre-specified convergence time Ts? Before answering this question, it is essential to know at this level what is the best value for n that corresponds to the optimum solution with Ts = 120 iterations. From Figure 4, it can be seen that n = 6 gives the optimum solution with Ts = 120. Similar results to those shown in Figure 3 and Figure 4 were obtained for the rest of the images in the dataset.

3 Discussion

First, we analyze the pre-specified convergence time effect. To do so, we repeated the above experiments with different T_s values. We realized that each value of T_s corresponds to a value of n, in Equation (2). When both values (T_s and n) are used together, they give local optima in the energy landscape of HNN.

Figure 5 shows the curves linking the convergence values of HNN with respect to the value of n in Equation (2) that are obtained with Ts values of 120, 60, and 30. We realized that the curves corresponding to T_s = 120 and T_s = 60 intersect in their optimum solutions obtained for n = 6, and the two curves are similar when n is integer in the range of 5–10.

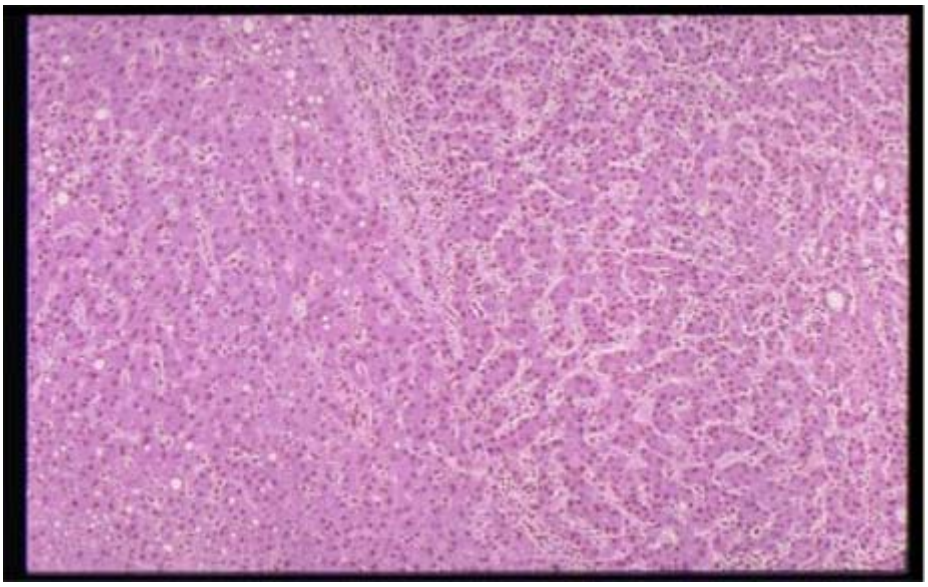

Figure 1: A sample of pathological liver colour image in true colour (Red, Green, and Blue). The cells' nuclei are represented by a circular shape shown in dark purple, the cytoplasm regions are coloured purple, the circular objects in white represent the fat cells, and the remaining objects in wave shape and white colour represent the fibrous tissues and blood sinus.

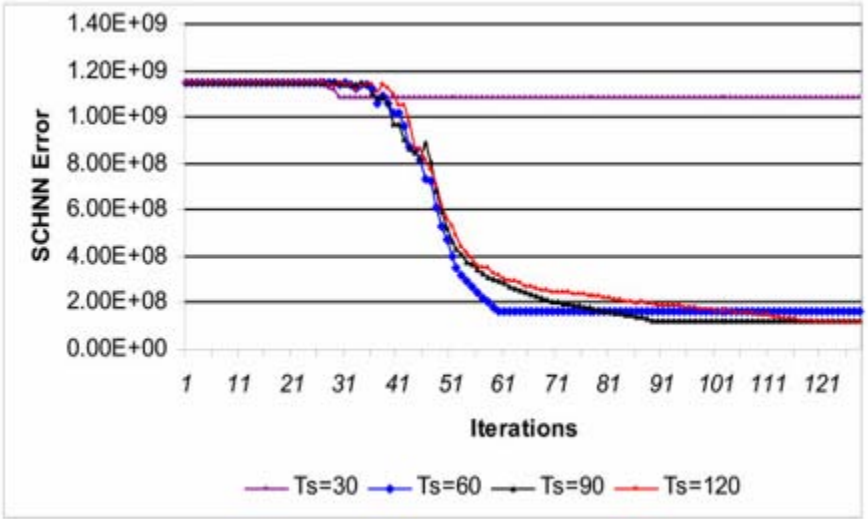

Figure 2. HNN energy function curves during the segmentation of the sample shown in Figure 1, using different values of the pre-specified convergence time T_s.

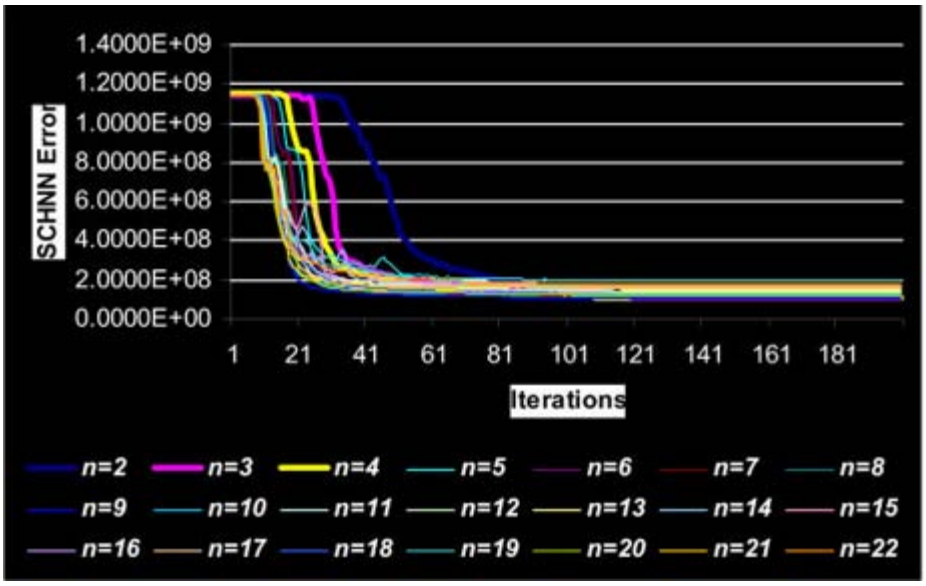

Figure 3. Different curves of the optimization of the energy function of the segmentation of the sample in Figure 1, as determined by considering different values of the variable n in equation (2) and with pre-specified convergence time Ts = 120 iterations.

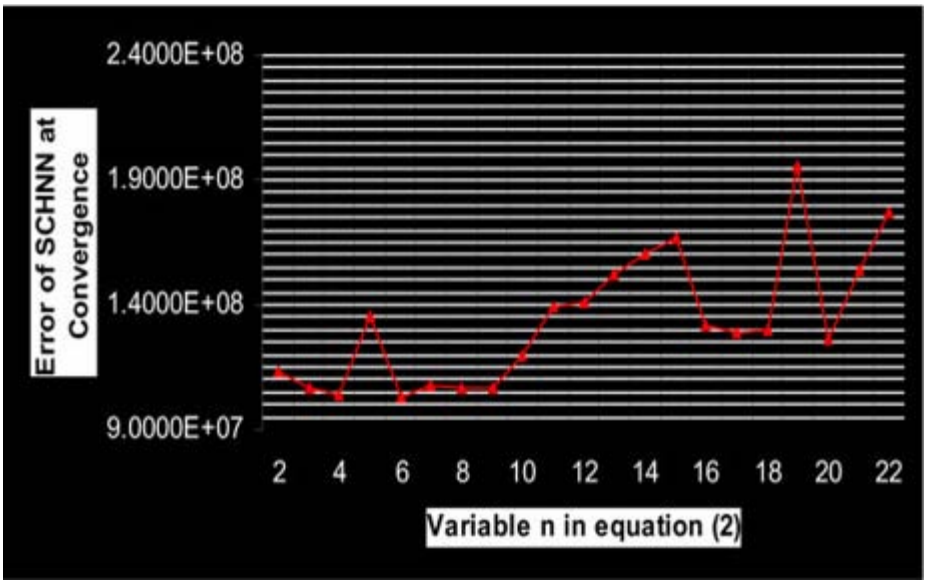

Figure4. This curve is extracted from Figure 3. It connects the convergence values of the energy function of the segmentation problem of the sample in Figure 1, by considering different values of the variable n in Equation (2), with the same random initialization matrix for all n values, and with a pre-specified convergence time Ts = 120 iterations.

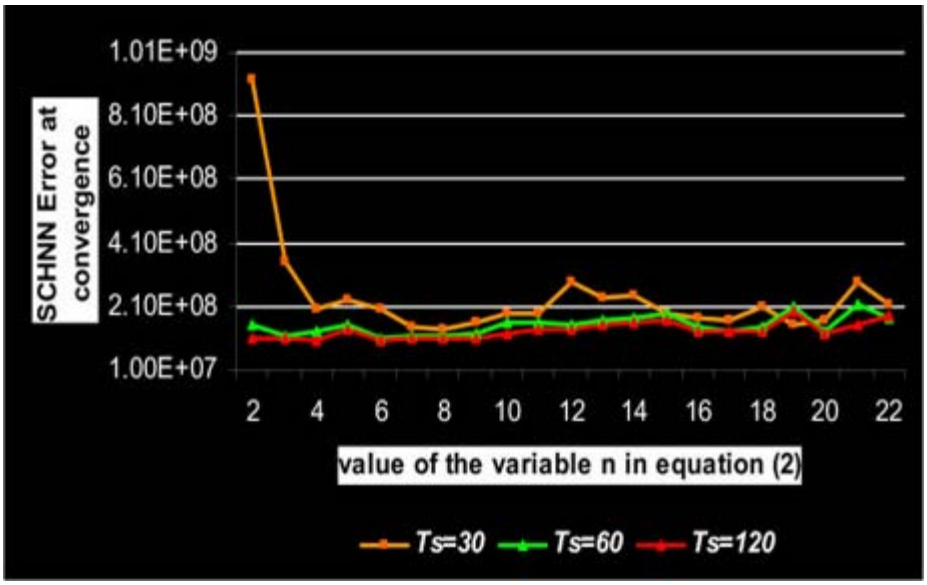

Figure5. Curves of the energy function of HNN at convergence with respect to values of the variable n in Equation (2) and for different pre-specified convergence times Ts. The green and red curves correspond to Ts = 60 and Ts = 120, respectively, are almost identical when *n* is an integer in the range of 5–10.

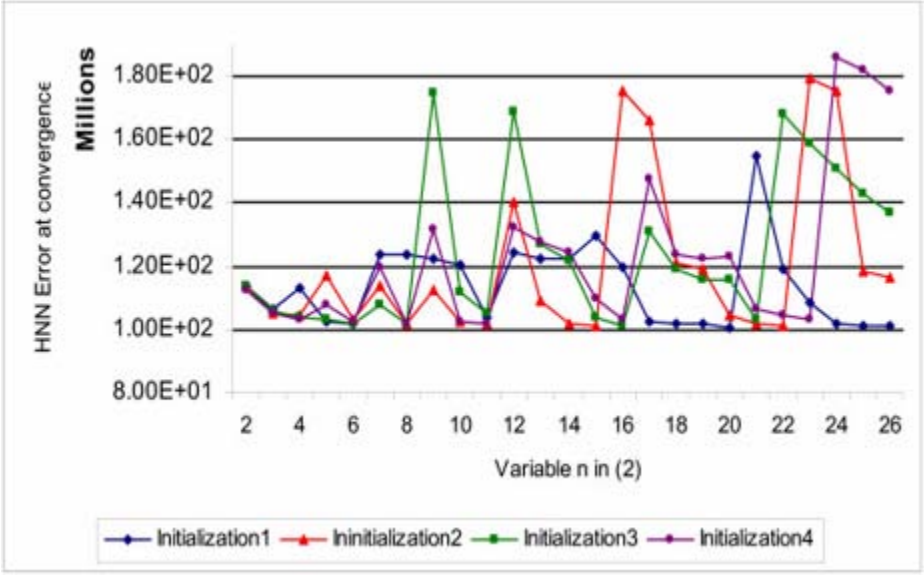

Figure6. Curves of the energy function of HNN at convergence with respect to values of the variable n in Equation (2) and for different initialization matrices.

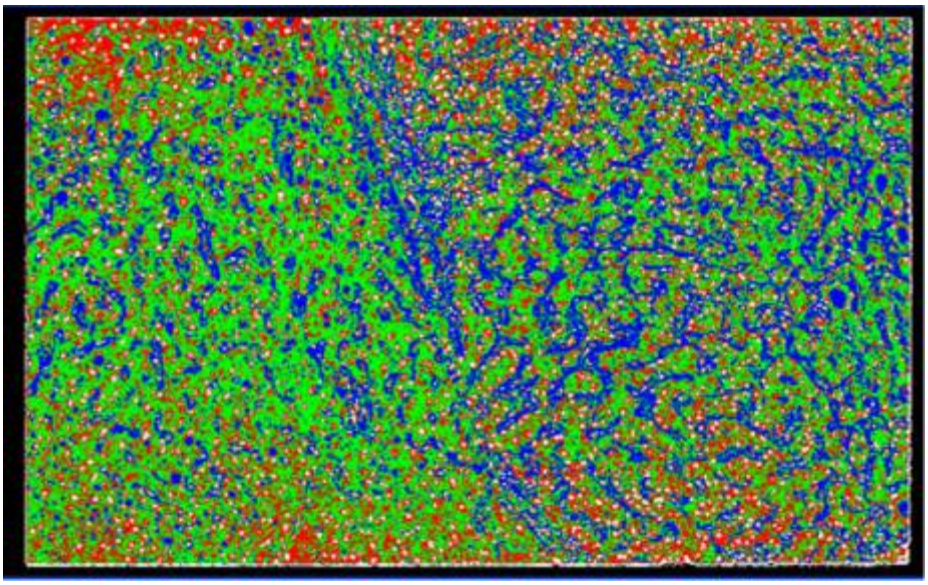

Figure7. Segmentation result of the sample in Figure 1, obtained using SCHNN in optimizing equation (1) with n = 2, and a pre-specified convergence time Ts = 120 iterations. The cells' nuclei are represented by a circular shape with white colour, surrounded by the red regions representing the cytoplasm of the cells, fat cells are coloured blue, and the fibrous tissues and blood sinus are coloured green.

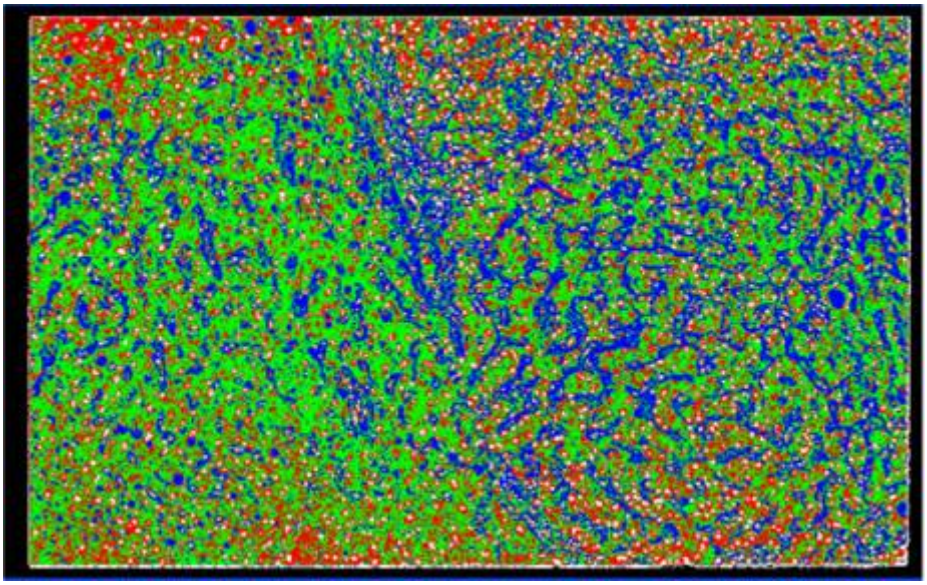

Figure 8. Segmentation result of the sample liver pathological image in Figure 1, obtained using SCHNN in optimizing equation (2) with n = 6, and a pre-specified convergence time Ts = 120 iterations. Colours are representative of those in Figure 7.

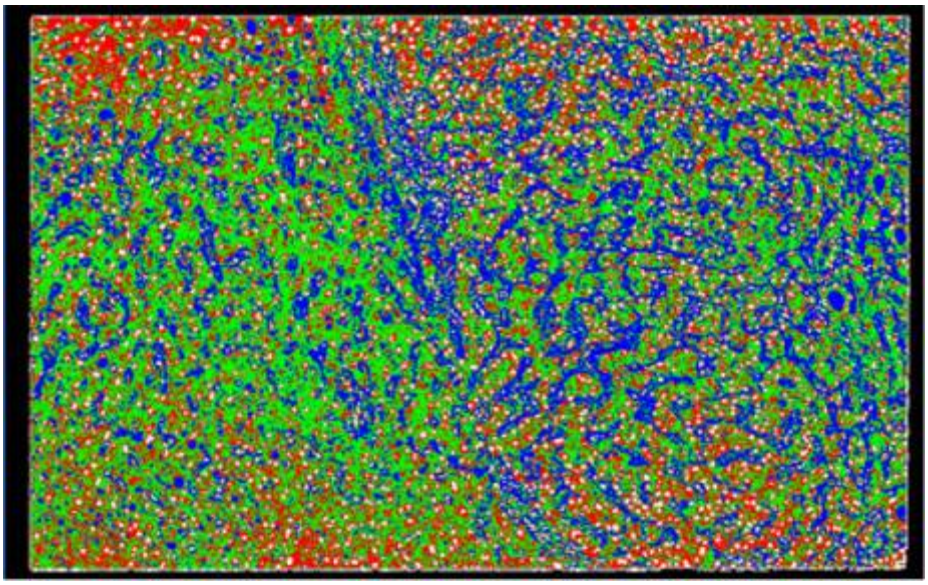

Figure 9. Segmentation result of the sample liver pathological image in Figure 1, obtained using SCHNN in optimizing equation (2) with n = 6, and a pre-specified convergence time Ts = 60 iterations. Colours are representative of those in Figure 7.

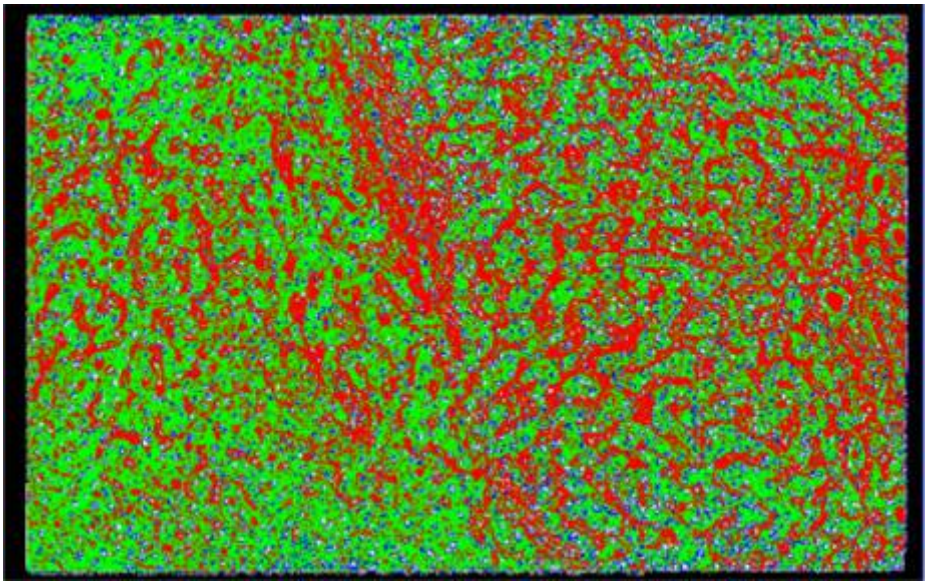

Figure10. Segmentation result of the sample liver pathological image in Figure 1, obtained using SCHNN in optimizing equation (2) with n = 12, and a pre-specified convergence time Ts = 30 iterations.

However, the curve corresponding to T_s = 30, shows higher error at convergence for all values of *n*.
Secondly, in order to analyze the HNN random initialization effect on the results of the algorithm described above, we have executed the same algorithm with different initialization matrices, and the curves of the convergence values of HNN corresponding to these initializations are shown in Figure 6. As is clear from the curves in Figure 6, the random initialization has no effect on the variable n in (2) when n = 6 where HNN gives an optimum and acceptable results that agree with the pathological experts' points of view. However, with other values of n, the random initialization may affect the solution to the problem, i.e., the error of the HNN at convergence as shown in Figure 6.

Figure7 shows the segmentation result of the sample in Figure 1, obtained using HNN in optimizing equation (1) with n = 2, and a pre-specified convergence time Ts = 120 iterations. The cells' nuclei are represented by a circular shape with white colour, surrounded by the red regions representing the cytoplasm of the cells, fat cells are coloured blue, and the fibrous tissues and blood sinus are coloured green.

Figure8 shows the segmentation result of the sample liver pathological image in Figure 1, obtained using HNN in optimizing equation (2) with n = 6, and a pre-specified convergence time Ts = 120 iterations. Colours are representative of those in Figure 7.

Figure9 represents the segmentation result of the sample liver pathological image in Figure 1, obtained using SCHNN in optimizing equation (2) with n = 6, and a pre-specified convergence time Ts = 60 iterations, also colours are representative of those in Figure 7.

Figure10 shows the segmentation result of the sample liver pathological image in Figure 1, obtained using SCHNN in optimizing equation (2) with n = 12, and a pre-specified convergence time Ts = 30 iterations. Colours are representative of those in Figure7.

By comparing the above described segmentation results, it is obvious that the results in Figures 7, 8, and 9 are similar to each other, however, in Figure10, the result is different in colouring and this because the tissues' clusters do not have the same density of pixels, which is translated by a high energy or (error) at convergence.

4 Conclusion

We analyzed the effect of considering the mean-square error in formulating the segmentation problem of multidimensional medical images. We have shown, empirically, that considering an integer power equal to six, of the error in the energy function of the problem, helped HNN to converge twice as fast as the same optimal solution obtained with the mean-square error algorithm. This result provides evidence that our segmentation method could prove useful for a Computer Aided Diagnosis (CAD) system for liver cancer and the like. In our future work, we will study in more detail the effect of the random initialization and its effect on the segmentation result and on the HNN classifier.

References:

[1] H. Ghabi-Oskoei, A. Malek, and A. Ahmadi: "Novel artificial neural network with simulation aspects for solving linear and quadratic programming problems", International Journal on Computers & Mathematics with applications Vol.53, 1439-1454, 2006.
[2] Chaney E and Pizer S: "Defining Anatomical Structures from Medical Images", Seminars in Radiation Oncology Vol.2, No. 4, 215-225, 1992.
[3] Tracton G, Chaney E, Rosenman J, Pizer S. Mask. "Combining 2-D and 3-D segmentation methods to enhance functionality", SPIE Conf Medical Imaging Bellingham, WA, 98-109, 1994.
[4] Brinkley JF., "A flexible, generic model for anatomic shape: Application to interactive two-dimensional medical image segmentation and matching", Computer Biomedical Resolution, Vol. 26, No. 2, 121-142, 1993.
[5] Lorensen W, Ferenc A, Kikinis R: The exploration of cross-sectional data with a virtual endoscope. In Interactive Technology and the New Paradigm for Health Care, Japan. IOS Press, 221-230; 1995.
[6] S.C. Orphanoudaki, C. Chronaki, and S. Kostomanolakis, "I/Sup 2/C: A system for the indexing, storage, and retrieval of medical images by content", Medical Informatics, Vol.19, 109-122, 1994.
[7] Humayun Karim Sulehria, YeZhang, "Hopfield Neural Network: Model,

Applications and Implementations", journal of WSEAS Transactions on Computer Research, Issue 2, Volume 2, February 2007.

[8] Sammouda R, Niki N, Nishitani H., "A Comparison of Hopfield Neural Network and Boltzmann Machine in Segmenting MR Images of the Brain, IEEE Transactions on Nuclear Science, Vol.43, No. 6, 1996.

[9] Amartur SC, Piraino D, Takefuji Y: "Optimization neural networks for the segmentation of magnetic resonance images" , IEEE Transactions on Medical Imaging, V.11, No.2, 1992.

[10] Sammouda M, Sammouda R, Niki N, et al., Liver cancer detection system based on the analysis of digitized color images of tissue samples obtained using needle biopsy. In International Journal of Information Visualization. Volume 1. Pagrave Press 2002.

[11] Fault Diagnosis for a Rolling Bearing Used in a Reciprocating Machine by Adaptive Filtering Technique and Fuzzy Neural Network", journal of WSEAS Transactions on Systems, Issue 1, Volume 7, February 2008.